THE ASTROPHYSICAL JOURNAL, 183: 237–264, 1973 July 1

THE OPTICAL APPEARANCE OF A STAR ORBITING AN EXTREME KERR BLACK HOLE*

C. T. CUNNINGHAM†
Department of Astronomy, University of Washington, Seattle
AND
JAMES M. BARDEEN
Department of Physics, Yale University, New Haven
Received 1972 December 5

ABSTRACT

Geometrical optics is used to analyze the propagation of high-frequency radiation emitted by a point source in a circular orbit in the equatorial plane of an extreme Kerr metric black hole. Both the apparent position and the energy flux of the brightest images as seen by certain distant observers are calculated as functions of time, taking into account the changing surface brightness of the image and its changing angular size. When the star's orbit is close to the black hole and the observer is close to the equatorial plane, the energy flux is sharply peaked in time. The correlation between direction of emission in the frame comoving with the source and the asymptotic direction of a beam of radiation gives the time-averaged energy flux as a function of polar angle. When the orbit of the source is close to the horizon in coordinate radius, most of the radiation comes out near the equatorial plane.

Subject headings: black holes — galactic nuclei — relativity

I. INTRODUCTION

Attempts to discover black holes must rely on the influence of their gravitational fields on nearby matter and/or their influence on the propagation of radiation in the vicinity of the black hole. Observable effects produced near the event horizon are particularly interesting, since they test strong-field predictions of general relativity.

One such effect is the modulation of high-frequency radiation emitted by a source which is in orbit about the black hole. The modulation is due to a combination of Doppler shifts, gravitational redshifts, and gravitational focusing. The first two effects determine the surface brightness of an image seen by a distant observer, while the last effect determines the apparent angular size of the image.

We envisage the source of radiation to be a star, with a mass the order of 1 $M_\odot$, in a bound circular orbit about the black hole. In order that the star not be tidally disrupted when it is in an orbit close to the black hole, the mass of the black hole must be considerably larger, particularly if the star is a white dwarf or ordinary main-sequence star. If M is the mass of the black hole, r_s is the coordinate radius of the star's orbit, and $\bar{\rho}$ is the mean density of the star, a crude criterion for the star to avoid tidal disruption is that the orbit lie outside the classical Roche limit:

$$r_s > (6M/\pi\bar{\rho})^{1/3} . \quad (1)$$

* Supported in part by the National Science Foundation (Grants GP-15267 and GP-32997X at the University of Washington and grant GP-36317 at Yale University) and in part by the Alfred P. Sloan Foundation.

† National Science Foundation Predoctoral Fellow.

Taking $\bar{\rho} = 10^{14}$, 10^{7}, and $1\ \mathrm{g\ cm^{-3}}$ as representative of neutron stars, white dwarfs, and main-sequence stars, respectively, the appropriate Roche limits are indicated in figure 1. The effects of the black hole on the radiation from the star are pronounced for $r_s \lesssim 20GM/c^2$.

The most likely location for a massive black hole ($M > 10^3\ M_\odot$) in a galaxy is in the galactic nucleus, as suggested by Lynden-Bell (1969). (See also Lynden-Bell and Rees 1971; Wolfe and Burbidge 1970.) Such a black hole is likely to have an angular momentum J near the maximum possible value for a Kerr black hole (Bardeen 1970),

$$J \lesssim GM^2/c\,. \tag{2}$$

The corresponding Kerr metric parameters are

$$a = J/Mc \lesssim m = GM/c^2\,. \tag{3}$$

For simplicity, and to maximize the effects of the rotation of the black hole, we consider the extreme Kerr black hole, for which $a = m$. Campbell and Matzner (1973) have independently made similar calculations for a Schwarzschild black hole, $a = 0$. A major difference between $a = 0$ and $a = m$ is the radius of the innermost stable circular particle orbit. When $a = 0$, stable particle orbits lie at radii $r > 6m$, where the geometry is not highly curved. However, when $a = m$, direct circular orbits in the equatorial plane are stable into $r = m$, the coordinate radius of the event horizon.

The orbits we consider are these direct circular orbits in the equatorial plane, with orbital angular momentum in the same direction as the angular momentum of the black hole.

The radiation from the star may be either electromagnetic or gravitational. As long as the frequency of the radiation ν obeys $\nu \gg c/m$, the geometrical-optics approxima-

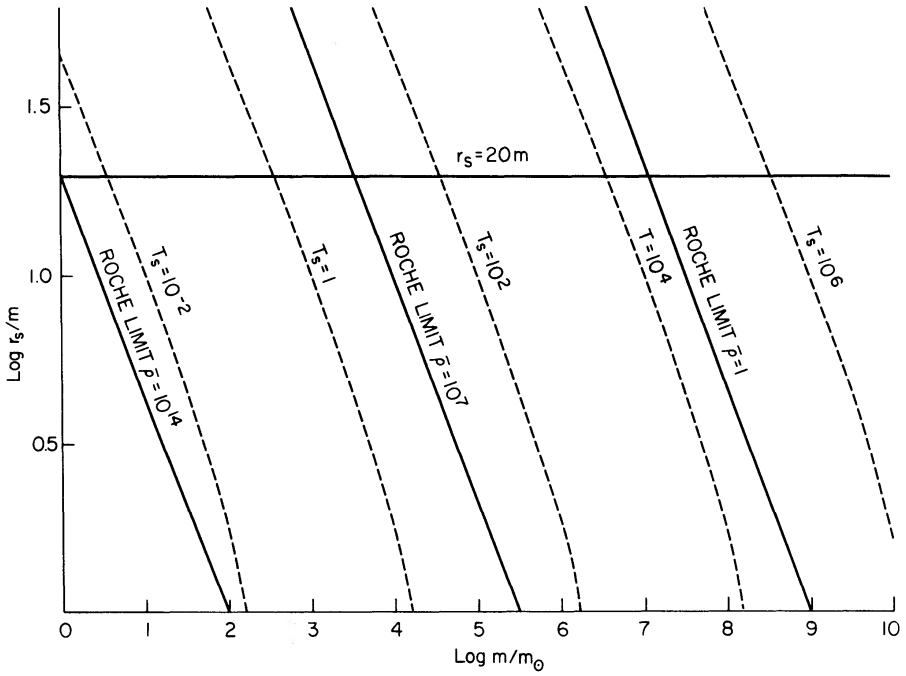

FIG. 1.—Roche limits for stars of mean density $\bar{\rho}$ ($\mathrm{g\ cm^{-3}}$) and orbital periods T_s(sec) as functions of the black hole's gravitational radius, $m = GM/c^2$, and the orbital radius r_s. Effects of the black hole on the star's radiation are pronounced for $r_s \lesssim 20m$.

tion is valid almost everywhere outside the black hole. We assume that the radiation is emitted isotropically and with a constant luminosity L in the local rest frame of the star. The change in the frequency of the radiation from ν_s in the local rest frame to ν_o far from the black hole determines the change in the intensity, or energy flux per steradian, I, of the radiation along each null geodesic between the surface of the star and the distant observer:

$$I_o = (\nu_o/\nu_s)^4 I_s \,. \tag{4}$$

There are an infinite number of null geodesics from the center of the star to the observer at any given time, since the "photon" trajectory can loop around the black hole any number of times. Each such trajectory gives a distinct image of the star on the celestial sphere of the distant observer. The energy flux F_o associated with a particular image is the product of the intensity I_o and the angular size of the image as seen by the observer. Generally only a few images will be significantly bright at any given time.

The apparent position and angular size of the image can be evaluated in terms of certain integrals along the trajectories of the photons. These integrals also give such information as the light travel time along the trajectory. The star is treated as a point source, in that the radius of the star is assumed to be infinitesimally small compared with the gravitational radius m of the black hole.

The basic description of the formalism we use is given in § II, though the details of the calculation of the angular size of the image are relegated to the Appendix. The results are discussed in §§ III–VI. First, in § III we consider the time-averaged photon (or graviton) fluxes and energy fluxes as functions of the asymptotic polar angle of the radiation. Time dilation and gravitational redshifts reduce the average fluxes below the Newtonian value everywhere except close to the equatorial plane, where the focusing of the radiation by the black hole is dominant. The time of emission for individual images and their positions seen by observers in the equatorial plane are discussed in § IV. In § V we show how the apparent positions of the images seen by observers out of the equatorial plane change with time. The dragging of inertial frames by the angular momentum of the black hole results in creation and destruction of images in pairs. Finally, in § VI we give the results of calculations of energy flux as a function of time for the few brightest images. The extent to which this is due to surface-brightness variations, as opposed to angular-size variations, is indicated. In the Conclusion, we mention some possible astrophysical applications of our results. Electromagnetic radiation from a source orbiting a massive black hole in the center of our Galaxy would have the best chance of detection in the radio or microwave region of the spectrum. The focusing of gravitational radiation from localized sources near a black hole into the equatorial plane of the Galaxy may be relevant for the interpretation of Weber's experiments.

II. DESCRIPTION OF THE PROBLEM

a) The Metric

It is convenient to use units such that $G = c = M = 1$, where M is the gravitational mass of the black hole. The unit of length is then $1.5 \times 10^{11}(M/10^6\ M_\odot)$ cm, or about 2 solar radii when $M = 10^6\ M_\odot$. The unit of time is $5(M/10^6\ M_\odot)$ sec. In these units the extreme ($a = m$) Kerr line element is

$$ds^2 = -e^{2\nu}dt^2 + e^{2\psi}(d\phi - \omega dt)^2 + e^{2\lambda}dr^2 + e^{2\mu}d\theta^2 \,, \tag{5}$$

with

$$e^{2\nu} = \frac{(r-1)^2(r^2+\cos^2\theta)}{[(r^2+1)^2-(r-1)^2\sin^2\theta]}, \tag{6a}$$

$$e^{2\psi} = \frac{[(r^2+1)^2-(r-1)^2\sin^2\theta]}{r^2+\cos^2\theta}\sin^2\theta, \tag{6b}$$

$$e^{2\lambda} = \frac{r^2+\cos^2\theta}{(r-1)^2}, \tag{6c}$$

$$e^{2\mu} = r^2+\cos^2\theta, \tag{6d}$$

$$\omega = \frac{2r}{[(r^2+1)^2-(r-1)^2\sin^2\theta]}. \tag{6e}$$

The physical interpretation of this line element is discussed by Ruffini and Wheeler (1971) and by Bardeen, Press, and Teukolsky (1972). The event horizon is at $r = 1$. In the ergosphere, the region $1 < r < 1 + \sin\theta$, the t-coordinate axis is in a spacelike direction, so real photons and test particles can have negative energies with respect to infinity. The function $\omega(r, \theta)$ describes the "dragging of inertial frames" by the angular momentum of the black hole. A photon or test particle with zero orbital angular momentum has an angular velocity $d\phi/dt = \omega$.

b) The Star's Orbit and Local Rest Frame

Denote the coordinate radius of the star's orbit by r_s. The angular velocity of the star's orbit in the equatorial plane of the black hole is

$$d\phi/dt = \Omega_s = \pm\frac{1}{r_s^{3/2}\pm 1}. \tag{7}$$

The upper signs refer to a direct (positive angular momentum) orbit; the lower signs, to a retrograde orbit.

We consider only direct orbits, which are stable for all $r_s > 1$; retrograde orbits are unstable for $r_s < 9$ and do not exist once $r_s < 4$. The period of revolution of the star, as seen by a distant observer, is indicated in figure 1 as a function of the black-hole mass and the star's coordinate radius.

To represent the local rest frame of the star we set up an orthonormal tetrad. The time leg of the tetrad is just the four-velocity of the star,

$$\Lambda_{(t)}{}^t = e^{-\nu}(1-V_s^2)^{-1/2} = \frac{r_s^{3/2}+1}{(r_s^{1/2}-1)(r_s^2+2r_s^{3/2})^{1/2}}, \tag{8a}$$

$$\Lambda_{(t)}{}^\phi = \Omega_s\Lambda_{(t)}{}^t = \frac{1}{(r_s^{1/2}-1)(r_s^2+2r_s^{3/2})^{1/2}}. \tag{8b}$$

The quantity

$$V_s = (\Omega_s-\omega)e^{\psi-\nu} = \frac{r_s^{3/2}+r_s+r_s^{1/2}-1}{(r_s^{1/2}+1)(r_s^{3/2}+1)} \tag{9}$$

is the velocity of the star in the locally nonrotating frame of reference (see Bardeen 1970; Bardeen *et al.* 1972). The ϕ-direction in the comoving frame is represented by a

unit spacelike vector $\Lambda_{(\phi)}{}^{\mu}$, orthogonal to $\Lambda_{(t)}{}^{\mu}$. The covariant components are

$$\Lambda_{(\phi)\phi} = e^{\psi}(1 - V_s^2)^{-1/2} = \frac{(r_s^{3/2} + 1)(r_s^{1/2} + 1)}{(r_s^2 + 2r_s^{3/2})^{1/2}}, \tag{10a}$$

$$\Lambda_{(\phi)t} = -\Omega_s \Lambda_{(\phi)\phi} = -\frac{r_s^{1/2} + 1}{(r_s^2 + 2r_s^{3/2})^{1/2}}. \tag{10b}$$

The remaining two space-axes in the comoving frame are chosen to be in the r- and θ-coordinate directions with

$$\Lambda_{(r)r} = \frac{r_s}{r_s - 1}, \tag{11}$$

$$\Lambda_{(\theta)\theta} = r_s. \tag{12}$$

c) *Photon Trajectories*

Carter (1968) has shown that the Hamilton-Jacobi equation governing geodesics in the Kerr metrics separates and that there is a complete set of constants of the motion from which the tangent four-vector can be calculated at any point along the trajectory. Two of the constants of the motion are directly generated by the symmetries of the metric. Interpreting the tangent vector to a null geodesic as the momentum four-vector of a photon (or graviton), these constants are the energy,

$$E = -p_t; \tag{13}$$

and the angular momentum about the axis of symmetry,

$$\Phi = p_\phi. \tag{14}$$

The third constant of the motion, Q, is related to p_θ by

$$p_\theta = [Q + E^2 \cos^2\theta - \Phi^2 \cot^2\theta]^{1/2}. \tag{15}$$

The trajectory of a photon is independent of its energy and may be described by the dimensionless parameters

$$\lambda = \Phi/E \tag{16}$$

and

$$q = Q^{1/2}/E. \tag{17}$$

The parameter q is real for all beams of radiation emitted by the star, as it is for all trajectories that intersect the equatorial plane.

The parameters λ and q are related to the direction cosines of a beam of radiation with respect to the ϕ-direction and the θ-direction in the local rest frame of the star. If Ψ is the angle of the beam with the direction of the star's motion (ϕ-direction) and Θ is the angle with the direction perpendicular to the equatorial plane [$(-\theta)$-direction],

$$\lambda = \frac{e^{\psi - \nu}(\cos\Psi + V_s)}{1 + e^{\psi - \nu}(\Omega_s \cos\Psi + \omega V_s)}, \tag{18}$$

$$q = r_s e^{-\nu}(1 - V_s^2)^{-1/2}(1 - \Omega_s \lambda)\cos\Theta. \tag{19}$$

The value of λ for a beam of radiation emitted by the star in the positive ϕ-direction ($\Psi = 0$) is

$$\lambda_+ = r_s + 1, \tag{20}$$

while the value associated with the negative ϕ-direction is

$$\lambda_- = -\frac{r_s^2 - r_s + 2}{r_s - 2}. \tag{21}$$

The angular momentum Φ associated with λ_- is always negative; the singularity in λ_- at $r_s = 2$ and the positive values when $r_s < 2$ are associated with zero and negative values of E. Needless to say, beams of radiation with $E \leq 0$ are necessarily trapped by the black hole.

While the photon trajectory associated with a given initial direction in the star's rest frame can be determined by integrating the tangent vector, the Hamilton-Jacobi method (Carter 1968) leads to the following equations, which take full advantage of the separation of variables. Let

$$\Theta(\theta) = q^2 + \cos^2\theta - \lambda^2 \cot^2\theta, \tag{22}$$

$$R(r) = r^4 + r^2 + 2r - 4r\lambda - r(r-2)\lambda^2 - (r-1)^2 q^2. \tag{23}$$

Then a photon trajectory which starts at $t = t_s$, $r = r_s$, $\theta = \theta_s$, $\phi = \phi_s$ goes to $t = t_0$, $r = r_0$, $\theta = \theta_0$, $\phi = \phi_0$ related by

$$\int_{\theta_s}^{\theta_0} \frac{d\theta}{[\Theta(\theta)]^{1/2}} = \int_{r_s}^{r_0} \frac{dr}{[R(r)]^{1/2}}, \tag{24}$$

$$\phi_0 - \phi_s = \Delta\phi = \mathrm{mod}_{2\pi}\left\{\int_{r_s}^{r_0} \frac{r(r-2)\lambda + 2r}{(r-1)^2[R(r)]^{1/2}}\, dr + \int_{\theta_s}^{\theta_0} \frac{\lambda \cot^2\theta}{[\Theta(\theta)]^{1/2}}\, d\theta\right\}, \tag{25}$$

$$t_0 - t_s = \Delta t = \int_{r_s}^{r_0} \frac{r^4 + r^2 + 2r - 2r\lambda}{(r-1)^2[R(r)]^{1/2}}\, dr + \int_{\theta_s}^{\theta_0} \frac{\cos^2\theta}{[\Theta(\theta)]^{1/2}}\, d\theta. \tag{26}$$

The integrals are understood to be path integrals along the trajectory. The signs of $[R(r)]^{1/2}$ and $[\Theta(\theta)]^{1/2}$ are always the same as the signs of dr and $d\theta$, respectively; the signs change at turning points in r or θ.

Given r_0, equations (24)–(26) determine θ_0, ϕ_0, and t_0 for given values of λ and q and given t_s, ϕ_s, θ_s, r_s. To find the values of λ and q associated with the images of the star seen by an observer at a given $r_0 \gg r_s$, at a given $\theta = \theta_0$, at $\phi_0 = 0$, and at a given time t_0, we note that the unknown ϕ_s and t_s are related by $\phi_s = \Omega_s t_s$, while $\theta_s = 90°$ and r_s is given. Thus,

$$0 = \mathrm{mod}_{2\pi}(\phi_s + \Delta\phi) = \mathrm{mod}_{2\pi}(\Omega_s t_0 - \Omega_s \Delta t + \Delta\phi) \tag{27}$$

provides one relation between λ and q, and equation (24) with $\theta_s = 90°$ and $r_0 = \infty$ provides a second. There is a denumerable infinity of pairs of values of λ and q which satisfy equations (24) and (27) for a given observer at a given time; each pair represents a single image of the star considered as a point source.

We classify the images according to the number of times the photon trajectory crosses the equatorial plane between the star and the observer. The trajectory of the "direct" image does not cross the equatorial plane; that of a "one-orbit" image crosses once; that of a "two-orbit" image, twice; etc.

d) Appearance of the Star

The apparent position of the image on the celestial sphere is represented by two impact parameters, α and β. These are measured relative to the direction to the center of the black hole (the radial direction for $r_0 \gg 1$). The impact parameter α is the apparent displacement of the image perpendicular to the projected axis of symmetry of the black hole, and β is the apparent displacement parallel to the axis of symmetry in the sense of the angular momentum of the black hole (see fig. 2). In terms of the conserved parameters λ and q

$$\alpha = -r_0 \frac{p^{(\phi)}}{p^{(t)}} = -\frac{\lambda}{\sin \theta_0}, \tag{28a}$$

and

$$\beta = \frac{r_0 p^{(\theta)}}{p^{(t)}} = [\Theta(\theta_0)]^{1/2} = (q^2 + \cos^2 \theta_0 - \lambda^2 \cot^2 \theta_0)^{1/2}. \tag{28b}$$

To calculate the frequency shift between the star and the observer, note that a photon (or graviton) with momentum four-vector p_μ has an energy in the local rest frame of the star

$$p^{(t)} = -\lambda_{(t)}{}^{\mu} p_\mu . \tag{29}$$

The ratio of energy (frequency) at infinity to energy (frequency) in the rest frame of the star depends only on λ,

$$g = E/p^{(t)} = (r_s^{1/2} - 1)(r_s^2 + 2r_s^{3/2})^{1/2}(r_s^{3/2} + 1 - \lambda)^{-1}. \tag{30}$$

When equation (18) is used to evaluate λ in terms of the direction cosine of the photon trajectory with respect to the ϕ-direction in the rest frame of the star, the result for g is surprisingly simple,

$$g = (r_s^2 + 2r_s^{3/2})^{-1/2}[(r_s^{1/2} + 1) \cos \Psi + r_s + r_s^{1/2} - 1]. \tag{31}$$

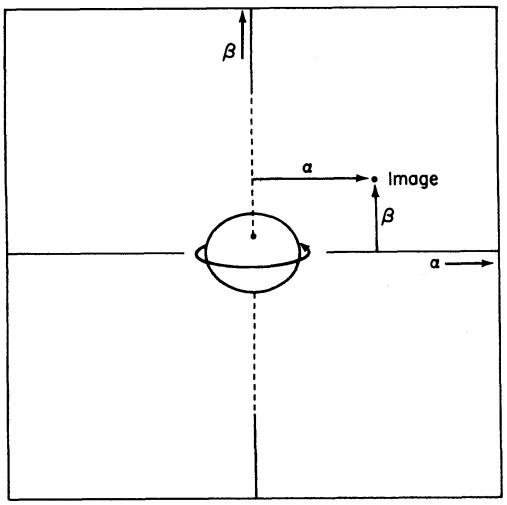

FIG. 2.—A small patch on the celestial sphere of a distant observer at radius r_0. The black hole is represented by a circle of unit radius, centered about the inward radial direction. The arrow indicates the direction of revolution of the orbiting star and the direction of rotation of the black hole about the axis of symmetry. The dotted line is the projection of this axis on the celestial sphere. The impact parameter α of an image seen by the observer is measured perpendicular to this projection; the parameter β, parallel to it.

The frequency shift varies smoothly with $\cos \Psi$ at all $r_s > 1$. There is always a net blueshift in the forward ϕ-direction, $\Psi = 0$, with

$$g_+ = (1 + 2r_s^{-1/2})^{1/2} . \tag{32}$$

The photon beam emitted in the backward ϕ-direction, with

$$g_- = (r_s - 2)(r_s^2 + 2r_s^{3/2})^{-1/2} , \tag{33}$$

corresponds to the maximum *observable* redshift only when $r_s > 4$. This beam is trapped by the black hole when $r_s < 4$.

The energy flux associated with a particular image seen by the observer is the product of the intensity I_0, the observed energy flux per unit solid angle, and the apparent angular size of the image. We assign the star a proper radius $b \ll 1$ and assume that the radiation is emitted isotropically from the surface.[1] Then in the rest frame of the star the intensity is

$$I_s = \frac{L}{4\pi^2 b^2} \tag{34}$$

for any beam of radiation that intersects the surface of the star. Geometrical optics tells us (see Lindquist 1966) that the intensity varies as the fourth power of the frequency along a beam of radiation, so

$$I_0 = g^4 I_s . \tag{35}$$

With no deflection of the null geodesic rays by the gravitational field of the black hole the apparent angular size of the star would be the Newtonian result, $\pi b^2/r_0^2$. The detailed calculation of the effects of gravitational focusing on the apparent angular size is given in the Appendix. We find the infinitesimal range of λ and q for which the trajectory intersects the star. This is converted to solid angle in the observer's frame of reference with the help of equations (28).

The result for the energy flux is presented as the ratio of the actual energy flux associated with the image to the "Newtonian" energy flux

$$F_N = I_s \pi b^2 / r_0^2 = L/(4\pi r_0^2) . \tag{36}$$

Both the intensity (surface brightness) and the angular size vary with time for a given image as the values of λ and q associated with the image change. Most of the time the angular size of an image associated with a photon trajectory which orbits the black hole a large number of times is extremely small relative to the Newtonian angular size, and such an image is negligibly faint.

III. TIME-AVERAGED FLUXES

Photon trajectories characterized by given λ, q are identical within additive constants in ϕ and t regardless of when the photons are emitted by the star. Therefore, the asymptotic polar angles θ_0, obtained from equation (24) with $r_0 = \infty$ for photon trajectories with various directions of emission in the local rest frame, are the only information needed for the time-averaged fluxes. The number of photons emitted per second per steradian in the local rest frame and the time-dilation factor between

[1] This is valid if the star radiates like a blackbody, for example. Podurets (1965) and Ames and Thorne (1968), in considering the optical appearance of a collapsing star in general relativity, assume a specific intensity at the surface of the star which varies as the secant of the angle between the beam and the normal to the surface, an assumption that leads to a physically unnatural infinite "limb brightening."

infinity and the local rest frame, $ds/dt = (U^0)^{-1}$, are both independent of the direction of emission. The average number of photons per second reaching infinity in a particular range of θ_0 is the product of those two factors with the solid angle in the local rest frame occupied by the corresponding photon trajectories. The only difference in calculating the general-relativistic correction to the average amount of energy per second reaching infinity in a given range of θ_0 is that the integral over solid angle in the local rest frame is weighted additionally by the frequency shift factor $g(\Psi)$ (eq. [31]).

The calculations are done graphically. For the photon flux, we plot curves of constant θ_0 on a projection of the hemisphere of photon trajectories in the local rest frame centered at $\Theta = 0$. The projection is such that the planar area is equal to the solid angle in the local rest frame; the radius R in plane polar coordinates is related to Θ by

$$R^2 = 2(1 - \cos \Theta) . \tag{37}$$

The hemisphere centered at $\Theta = \pi$ is identical in view of the reflection symmetry about the equatorial plane.

In flat space, with the star at rest, Θ would equal θ_0. However, the strong deflection of the trajectories near the black hole implies that there are an infinite number of closed curves in the plot for each value of θ_0, corresponding to the infinite number of times the photon trajectory can circle the black hole before it reaches the observer.

Figure 3 is such a plot for a star in orbit at $r_s = 1.5$. The region of trajectories trapped by the black hole is primarily in the backward ϕ-direction both because of the motion of the star relative to the locally nonrotating frame and because photons with positive angular momentum can escape more readily than those with negative angular momentum. The region occupied by direct photon trajectories (those which do not cross the equatorial plane) is compressed toward the outward radial direction. The one-orbit trajectories actually occupy more solid angle in the local rest frame than the direct trajectories in this case. The particular values of θ_0 chosen, such that

$$|\cos \theta_0| = 0.1, 0.2, \ldots, 0.9 ,$$

separate equal intervals of solid angle at infinity. The trajectories which cross the equatorial plane more than once (not shown) are squeezed between the one-orbit trajectories and those trapped by the black hole. The arrows by the curves indicate how the directions of emission of photon trajectories to the observer change with time as the star orbits the black hole, and the marks ◎ and ⊗ denote the directions of emission for the apparent creation and destruction of pairs of images (see the discussion in § V).

The relatively large area in figure 3 occupied by trajectories with $|\cos \theta_0| < 0.1$ indicates the degree of focusing of the photon flux toward the equatorial plane. The ratio of the total number of photons per second at infinity to the Newtonian value is the product of the fraction of the total area in figure 3 occupied by photon trajectories which reach infinity and the time-dilation factor $(U^0)^{-1}$. Since $U^0 \to \infty$ as $r_s \to 1$, the number of photons per second at infinity goes to zero in this limit, even though the fraction of photons trapped by the black hole is always less than 50 percent.

The solid angle in the local rest frame must be weighted by the frequency-shift factor $g(\Psi)$ in the calculation of the angular distribution of the time-averaged energy flux at infinity. This can also be done graphically if the two hemispheres in the local rest frame centered at $\Psi = 0$ and $\Psi = \pi$ are separately projected onto a plane in such a way that equal areas correspond to equal energy per unit time at infinity. For the forward hemisphere the plane polar radius R is related to Ψ by

$$\begin{aligned} R^2 &= 2\int_0^{\Psi} g(\Psi) \sin \Psi d\Psi, \; 0 < \Psi < \pi/2, \\ &= 4 \sin^2 (\Psi/2)(r_s^2 + 2r_s^{3/2})^{-1/2}[(r_s^{1/2} + 1) \cos^2 (\Psi/2) + r_s + r_s^{1/2} - 1] . \end{aligned} \tag{38}$$

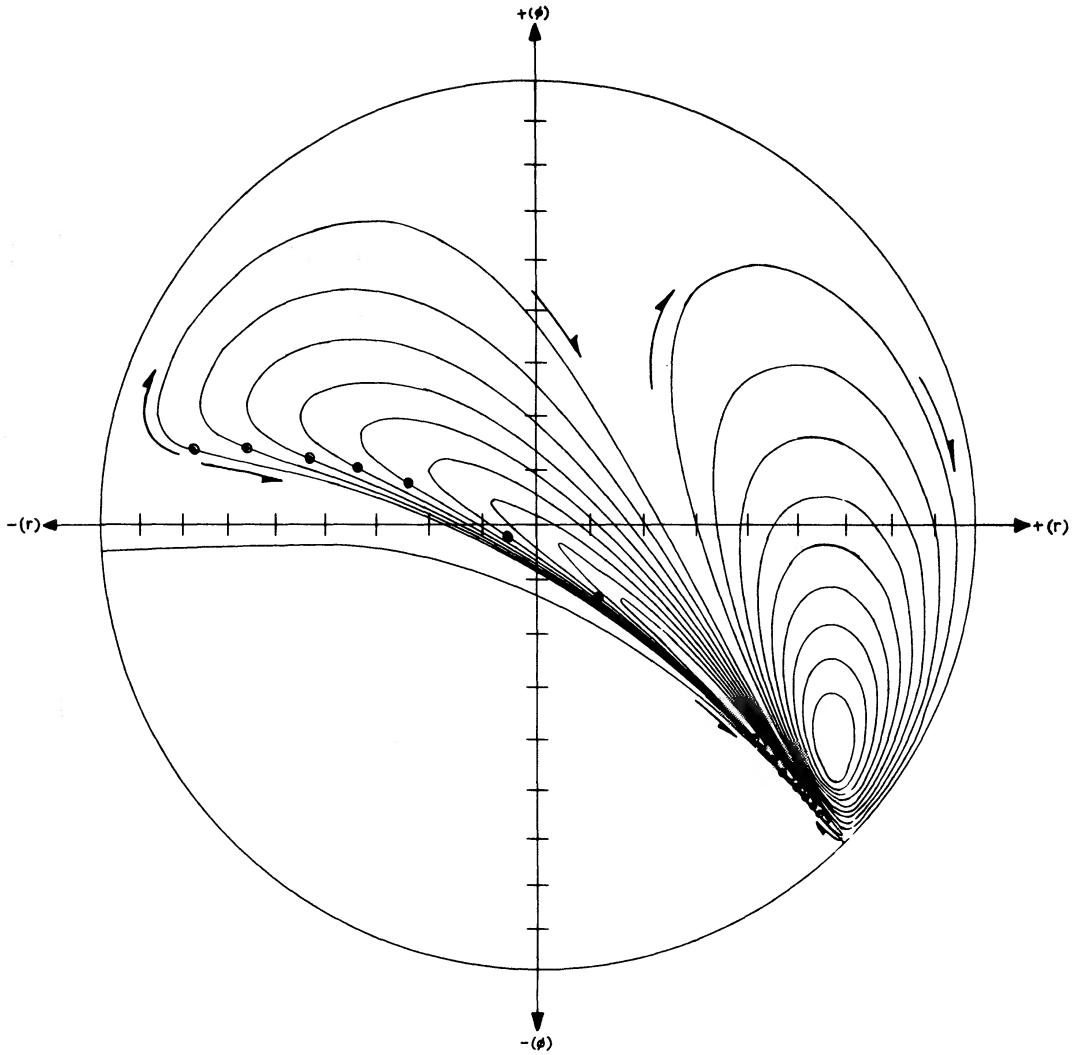

FIG. 3.—The asymptotic polar angle θ_0 as a function of the initial direction of a photon trajectory in the comoving frame for a star at $r_s = 1.5$. The plot is a projection of the upper ($\Theta \leq 90°$) hemisphere of photon trajectories such that unit area on the plot corresponds to unit solid angle in the comoving frame. It is used to determine the distribution of photon flux with polar angle far from the star. Tick marks on the axes indicate 10° divisions in Θ. The sets of nested, closed curves represent directions of emission for which $|\cos \theta_0| = 0.1, 0.2, \ldots, 0.9$, with the outermost curve in each set corresponding to $|\cos \theta_0| = 0.1$. The set nearer the outward radial direction represents direct trajectories; that nearer the inward direction, one-orbit trajectories. Directions of emission for multiple orbits lie between the region for one-orbit trajectories and the region for trajectories trapped by the black hole, the large, empty region containing the $-(\phi)$ (backward) direction. As the star orbits, image points representing directions of emission of photons to a stationary observer traverse a $\theta_0 =$ const. curve in the directions shown by the arrows. Curves representing one- and many-orbit trajectories are traversed partially clockwise, partially counterclockwise, with image pairs created at points ⊙, annihilated at points ⊗.

The backward hemisphere has $R = 0$ at $\Psi = \pi$ as long as $g(\pi) > 0$ ($r_s > 2$), but when the star is inside the ergosphere ($r_s < 2$) we set $R = 0$ at $\Psi = \Psi_1$, such that $g(\Psi_1) = 0$. The analytic formula is

$$R^2 = 4 \sin^2\left(\frac{\pi - \Psi}{2}\right)(r_s^2 + 2r_s^{3/2})^{-1/2}\left[-(r_s^{1/2} + 1)\cos^2\left(\frac{\pi - \Psi}{2}\right) + r_s + r_s^{1/2} - 1\right]$$

$$+ \left\{\begin{matrix} 0 & (r_s \geq 2) \\ \dfrac{(2 - r_s)^2}{(r_s^{1/2} + 1)(r_s^2 + 2r_s^{3/2})^{1/2}} & (r_s < 2) \end{matrix}\right\}. \quad (39)$$

The total energy per second reaching infinity between two values of θ_0 is the product of the corresponding planar area, the time-dilation factor $(U^0)^{-1}$, and the Newtonian luminosity per unit solid angle at infinity $L/4\pi$.

Figure 4 is the energy-flux plot corresponding to the photon-flux plot of figure 3. The star is at $r_s = 1.5$ and curves of constant θ_0 are shown for $|\cos \theta_0| = 0.1, 0.2, \ldots, 0.9$. Note that the focusing of the energy flux toward the equatorial plane is considerably enhanced over the focusing of the photon flux in this case, since the band between the direct trajectories and the one-orbit trajectories encompasses the forward ϕ-direction, where the factor g is the largest.

Planimeter measurements have been made of the area between neighboring values of θ_0 in figures 3 and 4, and similar diagrams for stars at $r_s = 3$, 7, and 20. Each such measurement gives the ratio of general-relativistic to Newtonian energy flux at infinity, averaged over solid angle in that range of θ_0. These ratios are plotted in figure 5. The general trend of the general-relativistic corrections to the angular distribution of the energy flux is evident. As r_s decreases, the energy flux near the poles becomes smaller and smaller relative to the average flux, primarily because the full gravitational redshift adds to the time-dilation effect for these trajectories. The mesh in θ_0 is not fine enough to show very well the large excess over the Newtonian flux near the equatorial plane due to the focusing of the radiation into the plane by the gravitational field of the black hole.

The ratio of the total luminosity of the star, summed over all directions at infinity, to the Newtonian value is easily calculated from diagrams of the type of figure 4. This ratio goes smoothly to zero as $r_s \to 1$, and is dominated by the time-dilation factor $(U^0)^{-1}$ (see fig. 6). The corresponding curve for the number of photons per second at infinity is virtually identical—the average frequency-shift factor g of the photons reaching infinity is close to one for all r_s.

IV. INDIVIDUAL IMAGES IN THE EQUATORIAL PLANE

As discussed briefly in § II, the parameters λ, q as functions of the observer's time are found with the help of integrals which give the travel time of the photon from the star to the observer, Δt, and the net change in the axial angle between the star and the observer, $\Delta\phi$. All these time-dependent quantities vary periodically, in the sense that the configuration of images seen by the observer is periodic with period $2\pi/\Omega_s$.

As a first step in exploring the properties of individual images we consider an observer precisely in the equatorial plane, at $\theta_0 = 90°$. For such an observer the direct, one-orbit, two-orbit, etc., labeling of the images is ambiguous, since the number of times the trajectory crosses the equatorial plane depends on whether the observer is infinitesimally above or infinitesimally below the plane. The primary distinction is between images in the equatorial plane (impact parameter $\beta = 0$) and images out of the equatorial plane.

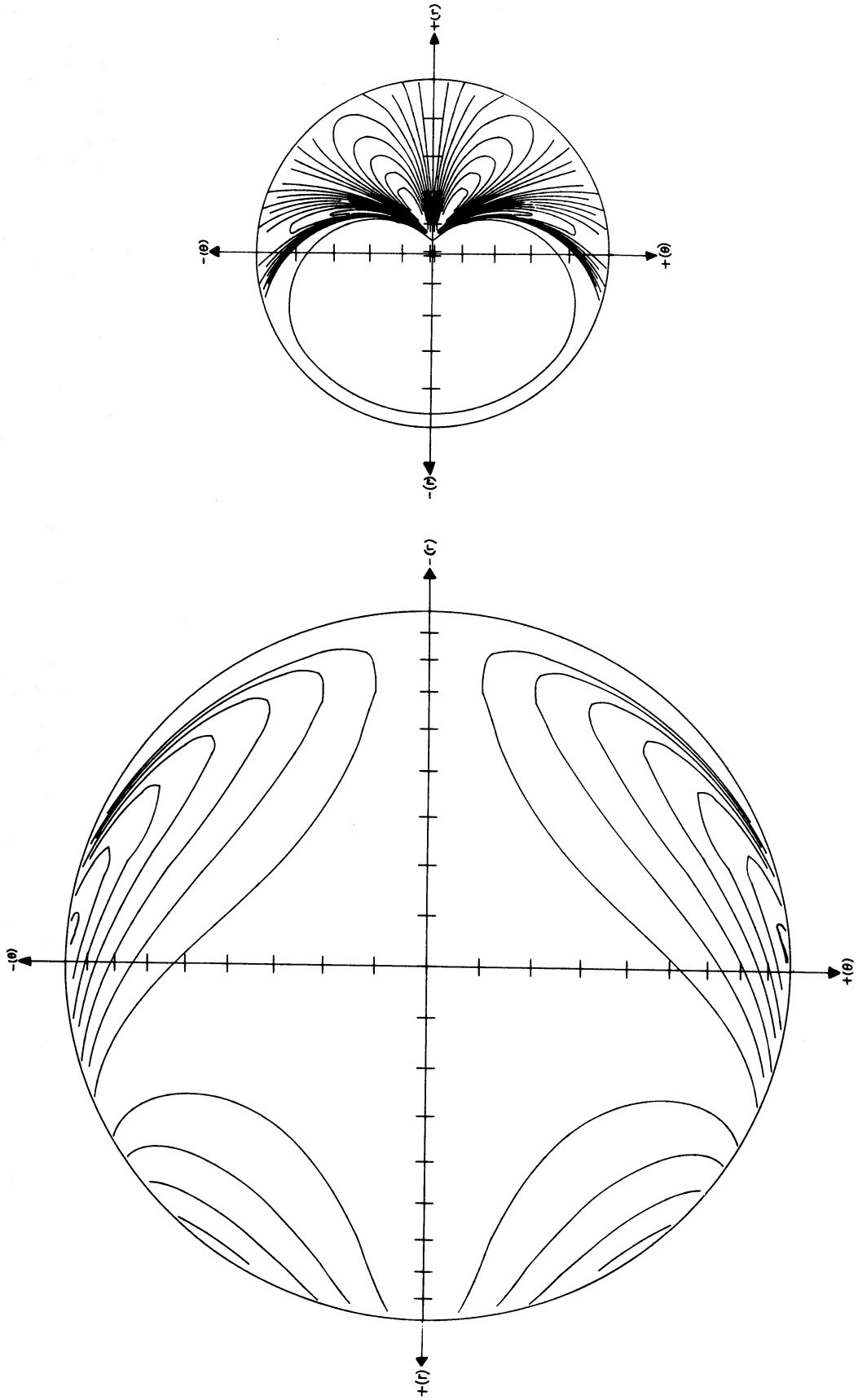

FIG. 4.—A plot of asymptotic polar angle as a function of initial direction, again for $r_s = 1.5$, but projected so that area on the plot is proportional to the product of the corresponding solid angle in the comoving frame and the frequency-shift factor $g(\Psi)$. This plot is used to obtain the distribution of energy flux with polar angle. The large circle represents the hemisphere of forward photon directions ($\Psi \leq 90°$); the small circle represents the backward hemisphere and contains the region for trajectories trapped by the black hole. Tick marks on the axes indicate 10° divisions in Ψ. Curves are given for $|\cos \theta_0| = 0.1, 0.2, \ldots, 0.9$, as in fig. 3. The large, open region about the forward direction ($\Psi = 0$) represents the flux carried along trajectories with asymptotic polar angles within 5°.76 of the equatorial plane; this is almost half the total luminosity of the star, measured over all polar angles at large distance.

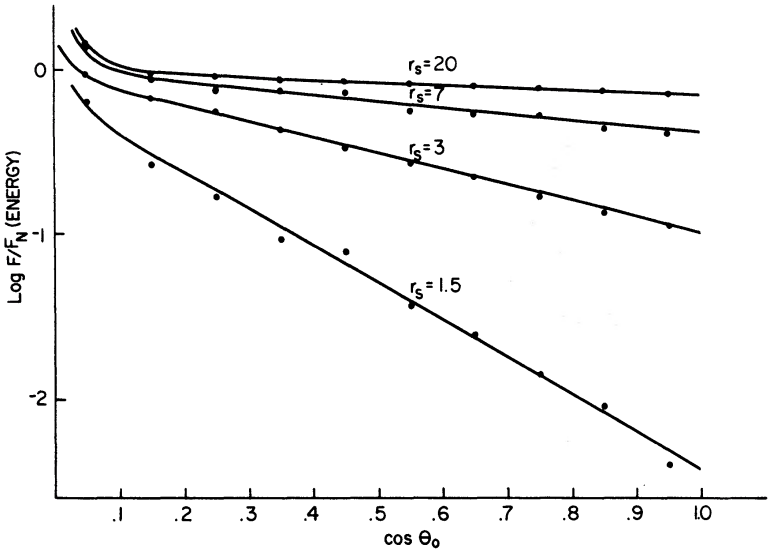

FIG. 5.—The distribution of energy flux from the star with polar angle, for stars at four orbital radii. The ratio of the observed flux F to the flat-space Newtonian value F_N was obtained from plots similar to fig. 4.

In figure 7 we consider the relation between time of emission and time of reception for images seen by an observer at $\theta_0 = 90°$, $\phi_0 = 0$, with the star at $r_s = 3$. The time of emission is

$$t_s = -\Delta\phi/\Omega_s + 2\pi n/\Omega_s\,, \tag{40}$$

where n is any positive or negative integer. The absolute phase relation between t_s and the time of observation is physically unimportant, since it depends on the precise value of r_0. We arbitrarily set $t_0 = 0 + 2\pi n/\Omega_s$ when $\lambda = 0$ for the image in the equatorial plane.

The solid lines show the relation between t_s and t_0 for trajectories lying entirely in the equatorial plane. Tick marks on these lines indicate the parameter λ and, hence,

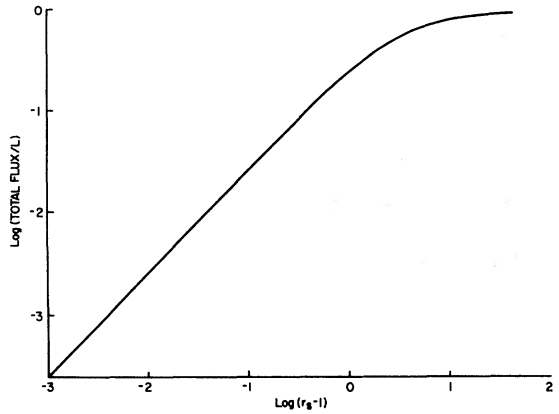

FIG. 6.—Ratio of the total luminosity of the star summed over all directions at infinity, to the luminosity L measured in the comoving frame, as a function of the star's orbital radius. The corresponding plot for the ratio of the number of photons per second measured at infinity to the number of photons per second measured in the comoving frame is virtually identical.

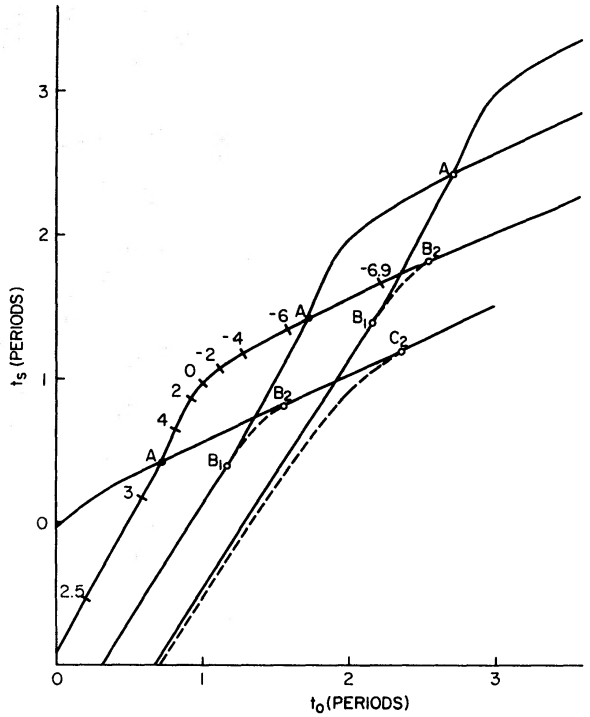

FIG. 7.—Time of emission t_s of photons from a star at radius $r_s = 3$ compared to their time of arrival t_0 at a distant observer directly in the equatorial plane ($\theta_0 = 90°$). Solid lines represent trajectories which stay entirely in the equatorial plane; dotted lines represent those which leave the plane. Tick marks on one of the solid lines indicate the parameter λ and, hence, the apparent positions of the images. Points A, B_1, B_2, C_1, C_2 mark times that images out of the plane split from or rejoin those in the plane. The flux from the images at these times is formally infinite. See text.

the observed position of the image. An image represented by one of the solid lines starts out with a trajectory which spirals around the black hole an infinite number of times in the $+\phi$-direction before escaping to reach the observer. The spiraling is close to the positive-angular-momentum circular photon orbit at $r = 1$. The angular velocity of the circular photon orbit is

$$\Omega_{\rm ph} = \tfrac{1}{2}\,. \tag{41}$$

During each orbit of the star the travel time of the photon trajectory decreases by $2\pi/\Omega_{\rm ph}$, since the trajectory corresponding to the given image must make one less circuit of the black hole in the ϕ-direction to reach the observer. Therefore,

$$\frac{dt_s}{dt_0} = (1 - \Omega_s/\Omega_{\rm ph})^{-1} = \frac{r_s^{3/2} + 1}{r_s^{3/2} - 1} \tag{42}$$

in the limit t_s, $t_0 \to -\infty$. In this epoch $\lambda \simeq 2$ and the image is almost stationary with $\alpha \simeq -2$.

Eventually the photon trajectory unravels completely and the image passes in front of the black hole. It is when the image crosses through $\alpha = 0$ (so $\lambda = 0$) that we set the phase of the observer's time equal to zero. Now the photon trajectory starts winding up again, this time at the retrograde circular photon orbit at $r = 4$ for which

$$\Omega_{\rm ph} = -\tfrac{1}{9}\,. \tag{43}$$

The travel time to the observer increases with each orbit of the star, and

$$\frac{dt_s}{dt_0} \to \frac{r_s^{3/2} + 1}{r_s^{3/2} + 10} \tag{44}$$

as t_s, $t_0 \to +\infty$. The value of λ for the trajectory approaches the value for the retrograde circular photon orbit, $\lambda = -7$, and the image becomes asymptotically stationary with $\alpha = +7$. The asymptotic slopes of the solid curves in figure 7 are in accordance with equations (42) and (44).

The dashed lines in figure 7 represent images which are seen by the observer to rise above or below the equatorial plane. At a point B_1 a pair of images separates from the image in the equatorial plane, one above the plane and one below. The images move to the other ($\alpha > 0$) side of the black hole and merge with a different equatorial plane image at a point B_2. The trajectories associated with these images cross the equatorial plane once between the star and the observer—since the observer is in the plane, these might be called "one and one-half orbit" images in our previous terminology. These images are due to photons which are emitted when the star is "in front" of the black hole and circle the black hole once before coming out to the observer.

Photons which are emitted out of the plane when the star is "behind" the black hole and reach the observer without any intermediate crossing of the equatorial plane are received at the isolated instants of time indicated by the points A in figure 7. At such an instant the observer sees a very bright "halo" around the black hole, which is the primary gravitational-lens effect of the black hole.

If the star were a Schwarzschild black hole the B_1–B_2 images would also appear as sudden instantaneous flashes to an observer in the equatorial plane. In the Schwarzschild case the properties of photon trajectories are independent of the *sign* of the angular momentum of the photon. The point B_1 is where a $\lambda > 0$ trajectory infinitesimally out of the equatorial plane is focused back into the plane after one crossing, and B_2 is the similar point for a $\lambda < 0$ trajectory. In the Schwarzschild case points B_1 and B_2 must coincide.

The spin-orbit coupling effect on photon trajectories in the Kerr metric means that in general $\lambda > 0$ and $\lambda < 0$ trajectories are not focused at the same time. For instance, the point C_2 is where trajectories are marginally focused with two crossings of the equatorial plane and $\lambda < 0$. The corresponding point C_1 for $\lambda > 0$ occurs so much earlier that it cannot be shown. The reason that the point C_1 occurs so much before the point B_1 along a given solid line is that when the trajectory is close to the horizon the time-dilation effect makes bending of the trajectory in the θ-direction very slow compared to the bending in the ϕ-direction generated by the dragging of inertial frames,

$$\frac{d\theta}{d\phi} = \mathcal{O}(e^{\nu} p^{(\theta)}/p^{(t)}) , \tag{45}$$

where here $p^{(\theta)}$ and $p^{(t)}$ are measured in a locally nonrotating frame of reference.

The remarkable thing is that the spin-orbit coupling does not spread out the focusing connected with the points A as it does with the points B, C, etc.

The energy flux received by the observer is formally infinite at points B_1, B_2, C_1, C_2, etc., as well as at point A. The image at these points is elongated by an infinite factor in the θ-direction, so the infinite surface brightness necessary to give a finite energy flux at the normal angular size gives an infinite flux. Of course, if the star is not idealized as a point source it has a finite surface brightness, and the angular size cannot increase by an infinite factor.

Figure 7 also indicates the times at which a sudden burst of radiation in the local rest frame would be seen by the observer. Whenever a horizontal line at the time t_s

intersects an image curve, the observer sees a flash of radiation at the corresponding time t_0.

V. APPARENT POSITION IN THE SKY

As soon as the observer is out of the equatorial plane, at $\theta_0 < 90°$, say, the ambiguity of the last section is removed. Now when the star is behind the black hole, the trajectories which go above the black hole without crossing the equatorial plane are definitely distinct from those which go below the black hole and must cross the equatorial plane once to reach the observer at $\theta_0 < 90°$. The gravitational focusing peak in the energy flux as a function of time associated with these trajectories and points of the type A in figure 7 decreases rapidly in height as $(90° - \theta_0)$ increases. However, focusing peaks corresponding to points of the type B_1, B_2, C_1, C_2, etc., remain as long as $\theta_0 > 45°$ or so.

In this section we present the apparent positions of the brightest images seen by observers fairly close to the equatorial plane ($\cos \theta_0 = 0.1$, $\theta_0 = 84°.24$) for stars at $r_s = 20$ and $r_s = 3$.

First consider an observer at $\theta_0 = 84°.24$ when the star is at $r_s = 20$. The star is close enough to the black hole so that relativistic effects are not so strong as to completely mask the conventional Newtonian picture. Figure 8*a* shows the motion in the (α, β)-plane for the two images with the greatest average brightness. The small, dashed circle is the locus $\alpha^2 + \beta^2 = 1$ and gives the scale of the drawing. This circle also corresponds to the appearance of a sphere of radius $r = 1$ at the same location as the black hole, but seen in flat space. The timing ticks labeled 0, 1, 2, . . . , 9 indicate the location of the image at 10 evenly spaced time intervals spanning one period of the star's motion, starting (at 0) when the direct image crosses the β-axis ($\lambda = 0$) in front of the black hole. The direct image follows the "actual" location of the star fairly well, except when the star is behind the black hole. As the star starts behind the black hole, the image lags behind (ticks 3, 4) and then very rapidly jumps over the black hole (ticks 5, 6). This rapid motion of the image corresponds to the gravitational focusing peak at a point like point A in figure 7. For an observer in the plane the image jumps instantaneously from one side of the black hole to the other.

The timing ticks for the one-orbit image are at identical times to those on the direct image curve. The one-orbit image is always strongly affected by the black hole. The rapid motion (ticks 5, 6) below the black hole is part of the same gravitational focusing peak as the rapid motion above the black hole of the direct image. Particularly interesting is the creation of a pair of images at point ◎ before timing tick 8. One of these images hovers near the equatorial plane near $\alpha = -2$ (corresponding to the segment B_1–A in fig. 7); the other moves in retrograde fashion above the black hole. The retrograde motion corresponds to the segment B_1–B_2 in figure 7. The retrograde one-orbit image meets the partner created with the previous retrograde one-orbit image, and the two images disappear at ⊗ (corresponding to point B_2), just after timing tick 9. This creation and destruction of images is intimately connected with the dragging of inertial frames and disappears when the angular momentum of the black hole is zero (see § IV).

Now consider figure 8*b* which is for an observer at $\theta_0 = 84°.24$ and a star at $r_s = 3$. The correspondence to figure 7 is more direct since the star's orbit is at the same radius. The star is inside the retrograde circular photon orbit, so as the star goes behind the black hole the direct image drifts outward before jumping over the black hole. At $r_s = 20$ the one-orbit image appears to remain close to the black hole compared to the direct image; at $r_s = 3$ this is reversed. For stars very close to the black hole the one-orbit image appears to move through a larger region of sky than does the direct image. As a result, both the maximum surface brightness (a function of λ, and there-

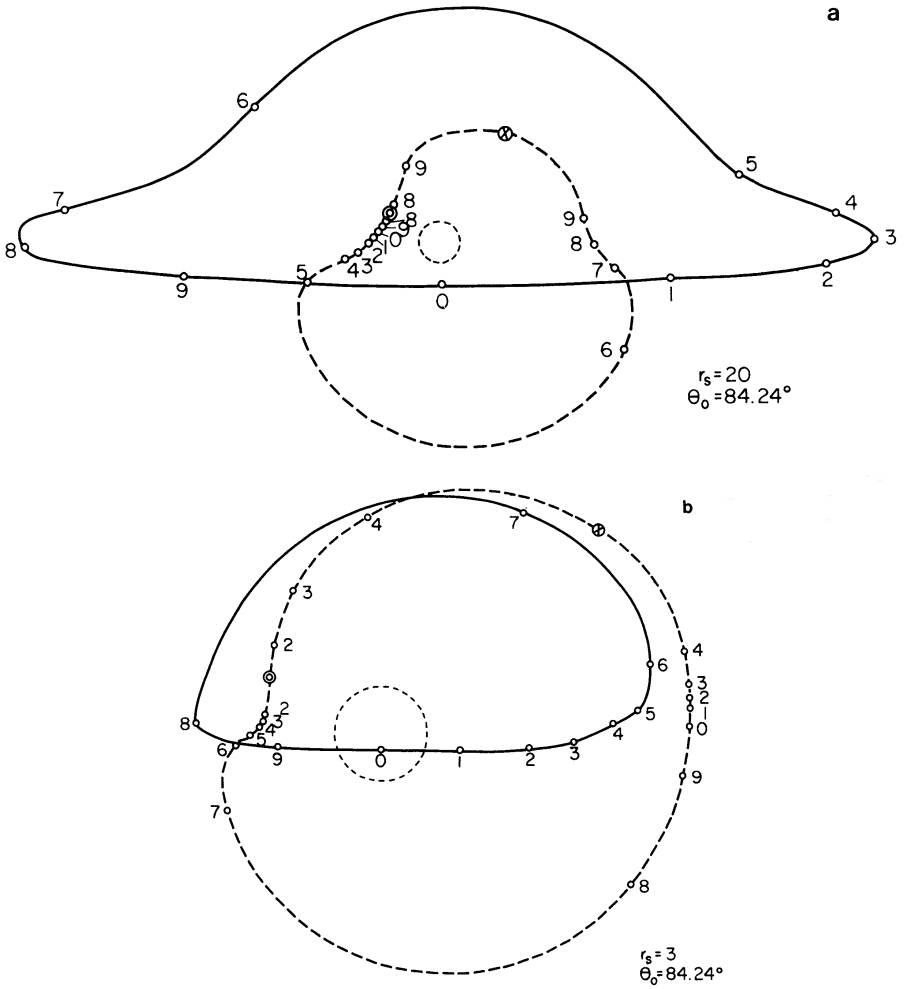

FIG. 8.—Apparent positions of the two brightest images as functions of time for two orbital radii and an observer at a polar angle $\theta_0 = 84°.24$. The small, dashed circle in each plot is the locus $\alpha^2 + \beta^2 = 1$ and gives the scale of the plot. The direct image moves along the solid line; the one-orbit image, along the dashed line. Ticks mark the positions of the images at 10 equally spaced times. A pair of one-orbit images appears to be created at the points ⊙ and annihilated at the points ⊗. See text.

fore of α) and the variation in surface brightness increase more rapidly for the one-orbit image than for the direct image as we consider stars of progressively smaller orbital radii.

As the apparent position of the image seen by the distant observer changes, so does the corresponding direction of emission in the local rest frame of the star. If the instantaneous direction of emission of the beam of radiation which reaches the observer is represented by a point in figure 3 (for $r_s = 1.5$), this point moves along the $\cos \theta_0 =$ const. curve corresponding to the given type of image in the direction indicated by the arrows. Creation of pairs of images on the one-orbit curves is at the points marked ◎; destruction, at points ⊗. For $r_s = 1.5$ there is no retrograde image and, hence, no creation and destruction of images for observers with $\theta_0 \lesssim 40°$.

When r_s is not much larger than unity, the images move very slowly on the parts of the curves nearest the backward ϕ-direction and very rapidly on the remainder of the

curves. During the rapid motion the images subtend relatively large solid angles in the local rest frame and have frequency shift factors $g \gtrsim 1$, while for the slow motion both the image solid angles and g are small. Therefore, the energy flux at the observer is very sharply peaked in time, as we shall see in § VI.

The direction of motion of the main image on each curve in figure 3 is clockwise. The secondary, retrograde, image on the one-orbit curves, which exists for $|\cos \theta_0| \leq 0.7$, moves in a counterclockwise direction. A similar pattern holds for two-, three-, and higher-orbit images. On the adjacent parts of the one- and two-orbit curves in the limit $\theta_0 \to 90°$ the images move in the same direction, so as we found in figure 7 the one- and two-orbit images which appear out of the plane as seen by an observer in the equatorial plane can last for a finite time. However, there is no retrograde image on the direct-orbit curves. In the limit $\theta_0 \to 90°$ the adjacent images on the one-orbit and direct curves move in opposite directions, but at the same time are degenerate. To an observer in the plane the radiation associated with the nonplanar direct and one-orbit combination *must* come in an instantaneous flash.

VI. LIGHT CURVES AND FREQUENCY SHIFTS

The observationally most relevant part of our calculation is the modulation of the energy flux by the black hole. As in the last section we show only the light curves for the direct image (*solid line*) and for the one-orbit image (*dashed line*). The method of calculation is given in the Appendix.

The energy flux as a function of time is shown in figures 9–12 for observers at $\cos \theta_0 = 0, 0.1, 0.5$ and stars at $r_s = 20, 7, 3, 1.5$. The time scale used is as in the previous sections: 10 units per period, $t_0 = 0$ at the reception of a $\lambda = 0$, direct-orbit photon. The light curves for an observer directly in the equatorial plane are somewhat incomplete, since only the energy flux from photons which stay entirely in the equatorial plane is shown.

From figures 9–12 some general features of the behavior of the energy flux with time are evident. The light curve of the direct image shows a main peak due to the changing surface brightness of the image. This peak is quite pronounced, even for $r_s = 20$, and becomes much higher and narrower for stars closer to the black hole; at $r_s = 1.5$ most of the flux arrives in a burst which has a duration of about 1/10 period. Effects of changing surface brightness are somewhat less pronounced for observers away from the equatorial plane. At about the time of the maximum in the main peak there is a peak corresponding to the primary gravitational focusing. This peak is infinitely high for observers in the equatorial plane but is very sensitive to the observer's polar angle and is relatively small even for $\cos \theta_0 = 0.1$. The star's orbital radius seems to have little effect on this peak.

The light curve of the one-orbit image shows a peak for the primary gravitational focusing at about the same time as does that of the direct image. As an observer moves away from the equatorial plane, this peak becomes smaller and shifts to earlier times, compared to the direct-image peak. The one-orbit light curve doubles back on itself at the times at which image pairs appear to be created and destroyed, an effect of a secondary gravitational focusing when the star is in front of the black hole. The energy flux is instantaneously infinite at these times; however, averaged over these peaks, the flux is substantial only for observers very close to the equatorial plane. As the observer moves off the equatorial plane, these infinite peaks move closer together and become narrower. For $\theta_0 \lesssim 45°$ they merge, giving one finite peak similar to that of the primary gravitational focus. The changing surface brightness of the one-orbit image is also important for determining its light curve. As the star's orbital radius decreases, this change in surface brightness becomes more pronounced. Also, the maximum surface brightness of the one-orbit image is greater than that of the direct image for

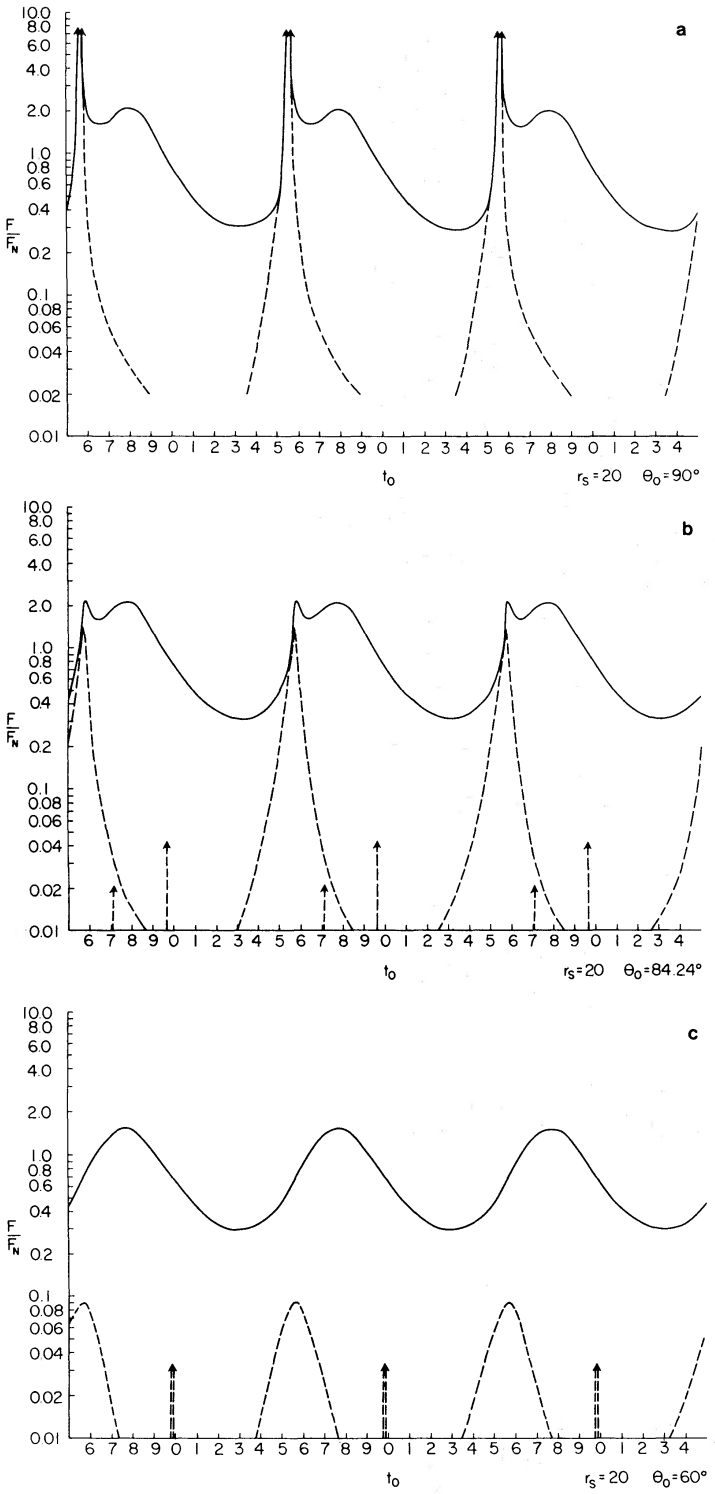

FIG. 9.—Light curves for the direct image (*solid*) and one-orbit image (*dashed*) of a star at $r_s = 20$, as seen by observers at three polar angles. Plotted is the ratio of the energy flux from the images F_0 to the Newtonian value for the flux, $F_N = L/4\pi r_0^2$, as a function of the observer's time. Fig. 9*a* is for an observer directly in the equatorial plane; peaks correspond to the primary gravitational focusing (of type A in fig. 7). The flux from trajectories which leave the equatorial plane and the narrow spikes associated with focusings of types B_1, B_2 in fig. 7 are not shown. Figs. 9*b* and 9*c* show complete direct and one-orbit light curves. The spikes in these figures mark focusings of type B_1, B_2, points at which the one-orbit light curve doubles back on itself.

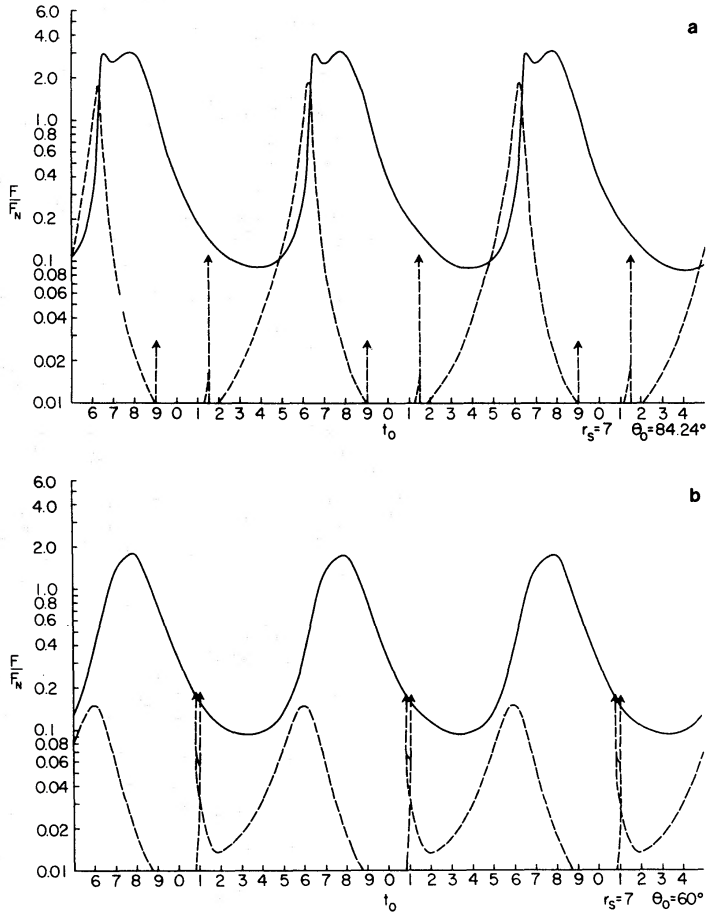

FIG. 10.—Light curves for a star at $r_s = 7$. They are very similar to those of fig. 9; however, the effects of changing surface brightness are more pronounced and the one-orbit images are brighter for this smaller orbital radius. Focusing effects appear to depend much more on the observer's polar angle than on the star's orbital radius.

$r_s \lesssim 2$; so that for stars very close to the black hole the one-orbit image produces more flux at the observer than does the direct image.

Thus the modulation of the energy flux from the star is produced by two factors: the changing surface brightness due to the Doppler effect of the star's orbital velocity, an effect which depends primarily on the star's orbital radius; and the changing image size due to gravitational focusing, which depends primarily on the angular position of the observer. These two effects may be separated by comparing figure 11*b*, the light curve for $r_s = 3$, $\cos \theta_0 = 0.1$, with figure 13, a corresponding plot of I_0/I_s, the ratio of the observed surface brightness of the images to that in the star's rest frame. Since

$$I_0/I_s = g^4 , \tag{46}$$

this plot also gives the redshift of the images as a function of time. We see that for $\cos \theta_0 = 0.1$ the primary gravitational focusing has a relatively small effect on the direct and one-orbit light curves and is responsible for changes of no more than a factor of 2 in the angular size of the images. Thus, the direct-orbit light curve and a large part of the one-orbit light curve are shaped primarily by the surface brightness. However, the secondary gravitational focusing when the star is in front of the black hole has a

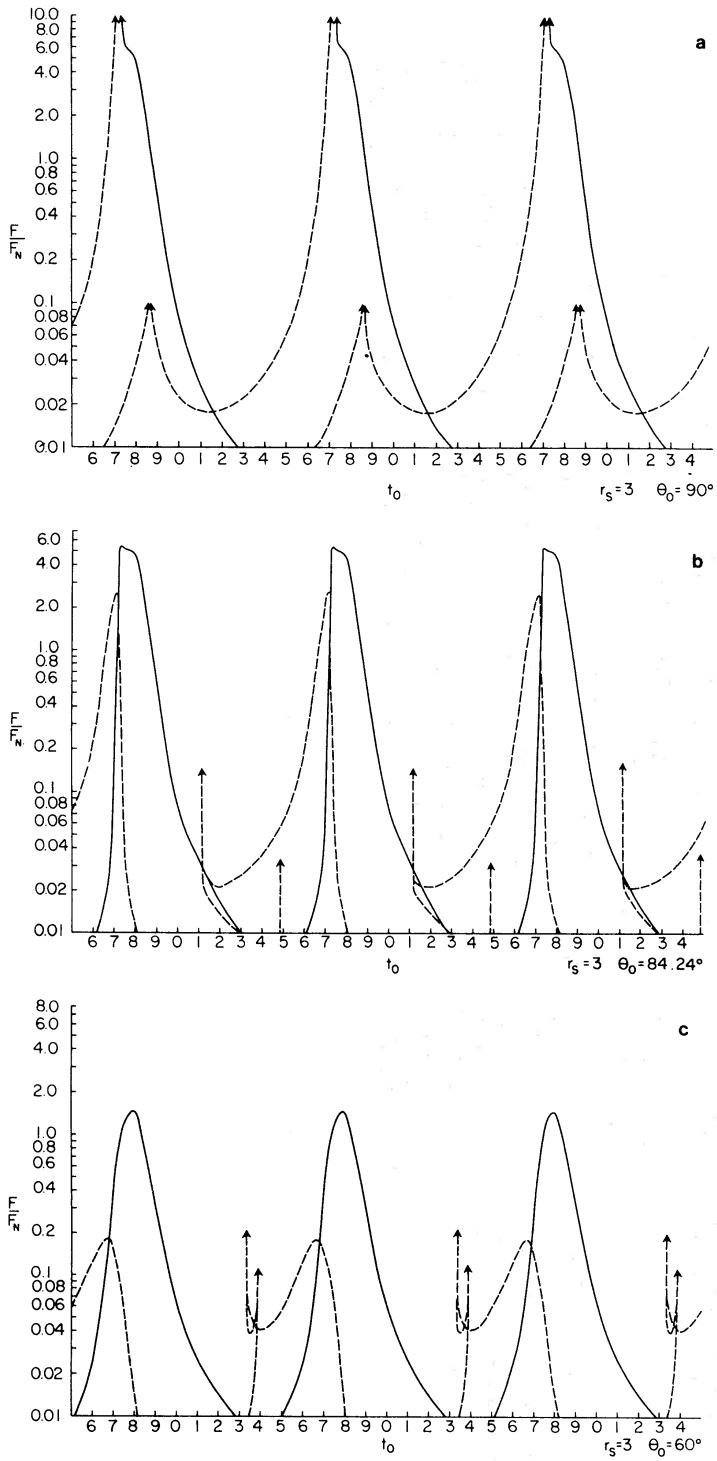

FIG. 11.—Light curves for a star at $r_s = 3$. The light from the star arrives in pulses due to the star's large orbital velocity. In fig. 11*a*, focusings of types A and B_1 are shown, and the flux from the two-orbit image (also shown as dashed) is appreciable at times. The two-orbit image is not shown in figs. 11*b* and 11*c*; these figures show the doubling-back of the one-orbit light curve clearly.

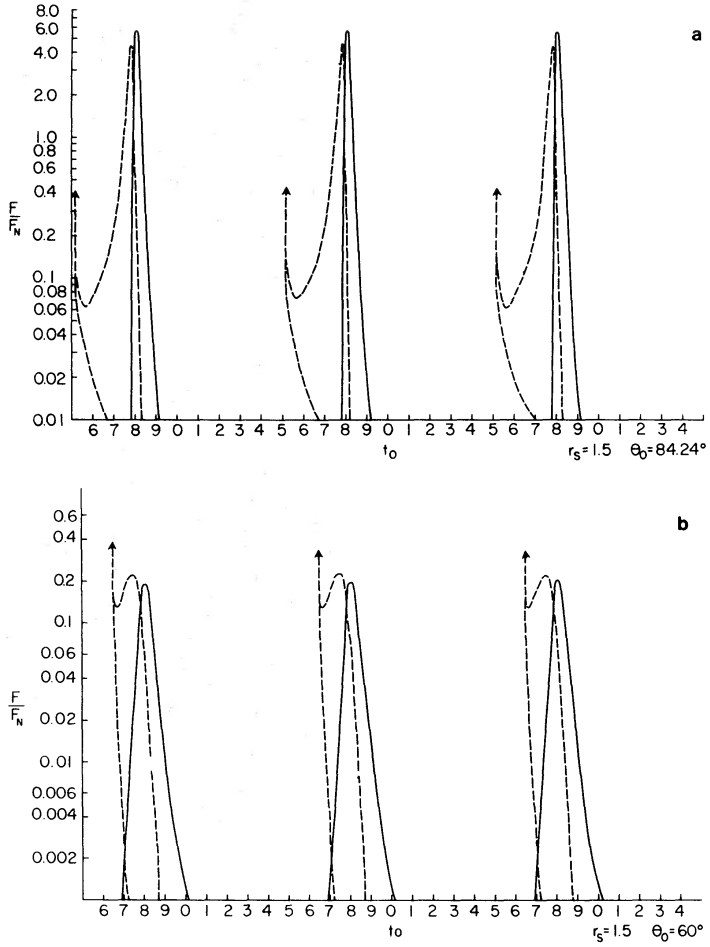

FIG. 12.—Light curves for a star at $r_s = 1.5$. The one-orbit image is generally brighter than the direct image in these figures. Note the decrease in flux for observers off the equatorial plane.

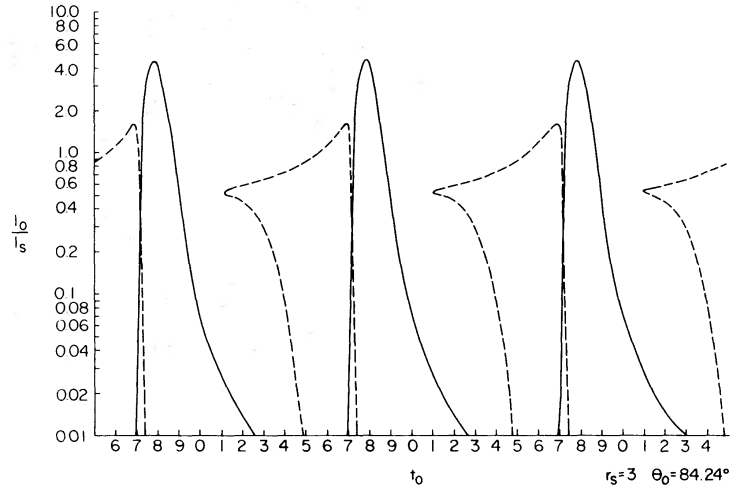

FIG. 13.—The ratio of the observed surface brightness I_0 of the direct image (*solid*) and the one-orbit image (*dashed*) to the surface brightness in the comoving frame I_s, for a star at $r_s = 3$, an observer at $\theta_0 = 84°.24$. Comparison with fig. 11*b* shows the effects of focusing on the image's angular size.

great effect on the one-orbit light curve, causing it to double back on itself, and produces large changes in its amplitude.

VII. SUMMARY AND CONCLUSION

The effects we have calculated are quite striking, and if they could actually be observed they would provide detailed, unambiguous information on strong-field predictions of general relativity. Relativistic effects are also quite important in neutron stars, for instance, but here the uncertainties in the nongravitational physics of the equation of state, the magnetosphere, etc., are likely to mask the details of the relativistic corrections for some time to come.

The motion of the images in the plane of the sky of a distant observer is quite nonuniform when the source of the radiation is close to the black hole, and is marked by the creation and destruction of pairs of images. The latter effect is a direct consequence of the dragging of inertial frames produced by the rotation of the black hole. The symmetry between trajectories which circle the black hole in opposite directions is broken, so, for instance, one-orbit images of positive angular momentum are not created at the same time that one-orbit images of negative angular momentum are destroyed. Unfortunately, it seems unlikely that effects which depend on resolving the individual images can actually be observed. For a black hole in the center of our Galaxy an impact parameter of $5m$, roughly the radius of the apparent motion of a multiple-orbit image, corresponds to an angle of $6 \times 10^{-6}(M/10^6\ M_\odot)$ arc seconds. This angle is only marginally resolvable with current radio techniques when the black-hole mass is at its observational upper limit of about $10^8\ M_\odot$ (see Lynden-Bell and Rees 1971).

The strong modulation of the energy flux shown in figures 9–12 is relatively easy to detect, even in the presence of considerable background radiation, because it is periodic. The primary cause of the modulation is the variation in surface brightness of the images, rather than gravitational focusing, unless the observer is very precisely in the equatorial plane (the plane of the orbit of the star). The peaks in the energy flux as a function of time are extremely sharp, even when r_s is as large as $1.5m$.

Most of the radiation comes out with a frequency-shift factor g the order of one. The bulk of the radiation received by a distant observer, even if it is emitted over a range of coordinate time $\Delta t_s \sim \pi/\Omega_s$, is received at infinity over a range of coordinate time $\Delta t_0 \sim \Delta t_s/U^0$, since $g \sim 1$ implies that the ratio of proper time at infinity to proper time in the comoving frame is the order of one. Thus the bulk of the energy reaching infinity comes out in at most a fraction $1/U^0$ of the period of revolution of the star.

The average frequency-shift factor g and the amplitude of the pulsing of the observed flux decrease as the observer's angular distance from the equatorial plane increases. If the observer is on the axis of symmetry, the energy flux is independent of time and the frequency-shift factor $g = 1/U^0$ for all trajectories reaching the observer. When the star is close to the black hole, most of the radiation emitted by the star is bent toward the equatorial plane, which, combined with the small g, makes the energy flux received near the axis of symmetry very small compared with the average flux near the equatorial plane.

The gravitational-lens effect is important when the observer is very close to the equatorial plane. All the photons emitted on the boundary between the direct and one-orbit regions in figure 3 are received in a single instant by an observer precisely in the equatorial plane. Relatively minor gravitational focusing peaks occur when pairs of images are created or destroyed, and these persist for observers up to 30° away from the equatorial plane. Of course, if the trajectory associated with an image circles the black hole several times near a "circular" photon orbit, the image is very strongly defocused and has negligible intensity.

Our calculations have not been extended to a star orbiting at a radius $r < 1.5m$ because it seems unlikely that such an orbit can be realized for an astrophysically plausible black hole. The radius of the innermost stable circular orbit increases rapidly as a/m decreases from one, $(r - m)/m \sim [4(1 - a/m)]^{1/3}$. A black hole with a/m precisely equal to one is unstable to dynamical perturbations, since there is an infinitely long (in proper distance) "tube" at $r \sim m$ composed of marginally trapped surfaces (see Bardeen, Press, and Teukolsky 1972). Any dynamical perturbations will convert these into trapped surfaces, moving the event horizon out to $r > m$, and will correspondingly decrease a/m. Our results for $a/m = 1$ should apply as long as a/m is fairly close to one and r_s is larger than the radius of the innermost stable circular orbit.

In the limit $r_s - 1 \ll 1$ we expect that several multiorbit images will dominate the energy flux received at infinity, and that the energy flux for each image will be sharply peaked in time. While the one-orbit and direct peaks approximately coincide when $r_s = 1.5$, we do not know whether the peaks for the bright images will coincide or be distributed uniformly in time when r_s is very close to one.

Even if a massive black hole does exist in the nucleus of our Galaxy or a neighboring galaxy, the chance that a star is in a close orbit about the black hole at any given time is probably not very large. Wolfe and Burbidge (1970) have tried to estimate the rate at which stars are accreted by a black hole in the nucleus of an elliptical galaxy; they find that even for a $10^8\ M_\odot$ black hole the rate is probably not more than one star every 300 years. The amount of time a star spends in a close orbit can be estimated from weak-field formulae for gravitational radiation from binary systems (Peters 1964). If M is the mass of the black hole, the time scale associated with the decay of an orbit of a star of mass M_* is

$$t_d \sim \left(\frac{r}{M}\right)^4 \left(\frac{M}{M_*}\right)^2 \left(\frac{M_*}{M_\odot}\right) \times 10^{-7} \text{ seconds} \tag{47}$$

(adapting a formula given in Misner, Thorne, and Wheeler 1973). A lifetime of one year with $r/M = 3$, $M_* = M_\odot$ requires $M \sim 2 \times 10^6\ M_\odot$.

The large amount of extinction along the line of sight to the Galactic nucleus makes observations in optical frequencies effectively impossible. In any case, a normal star that is bright optically has a relatively large radius and will be broken up by tidal forces before getting close to the black hole, unless the black-hole mass is rather unreasonably large. On the other hand, a neutron star emitting pulsed radio waves (a pulsar) could be detected at the distance of the Galactic nucleus and perhaps offers the best hope of seeing the effects described in this paper. For a black hole of mass $\sim 10^6\ M_\odot$ the pulsar would act as a good point source. The period of the radio bursts from the pulsar would be small compared to the period of revolution around the black hole.

Given the current uncertainties about conditions in galactic nuclei, particularly if Weber's observations of gravitational waves from the nucleus of our Galaxy (Weber 1970) are confirmed, any estimate of the probability that a point source is close to a massive black hole in the nucleus must be considered as no more than a guess. Partridge (1971) has looked for microwave radio bursts coincident with Weber's "gravitational wave" events, and it would seem worthwhile to analyze the microwave data for periodicities of the sort suggested here.

The solar system is close enough to the galactic plane for gravitational focusing to increase the peak energy flux considerably above Newtonian values, assuming that the equatorial plane of the black hole is the same as that of the Galaxy. Campbell and Matzner (1973) have suggested that such focusing effects on the gravitational radiation from a localized source near a massive black hole might ease the energy requirements

associated with Weber's events, and they have made quantitative estimates for a Schwarzschild black hole.

Another context in which our results might be useful is when a black hole of about 10 $M_\odot$ is in a close binary system and is accreting gas from a companion star. There is some observational evidence that the Cygnus X-1 X-ray source is such a system (Webster and Murdin 1972). The accreting material is likely to form a disk around the black hole. The rapid time variations in the X-ray output from Cygnus X-1 might be due to time-varying Doppler shifts from localized "hot spots" in the disk (Shakura and Sunyaev 1972). The size of a "hot spot" is likely to be on the order of the radius of the black hole, so our point-source approximation may not be entirely appropriate.

APPENDIX

CALCULATION OF THE ENERGY FLUX

Consider a particular image of the star, for which the photon trajectory passing through the center of the star is located at impact parameters (α_k, β_k) which are functions of time. There are corresponding values (λ_k, q_k). An exact calculation would allow for the finite size of the star (proper radius b in the local rest frame) and find the precise range of impact parameters about (α_k, β_k) for which the photon trajectories still intersect the surface of the star.

The energy flux F_0 measured by the observer is the integral of the surface brightness over the angular spread of the image. The element of solid angle is $d\alpha d\beta/{r_0}^2$. The specific intensity is given by equations (34) and (35). Therefore,

$$F_0 = \iint \frac{d\alpha d\beta}{{r_0}^2} \frac{L}{4\pi^2 b^2} g^4 . \tag{A1}$$

We only expand to first order in the deviation of the photon trajectory from the central one. In this approximation g is uniform over the image, and

$$F_0 = \frac{L}{4\pi^2 b^2 {r_0}^2} g(\lambda_k)^4 \iint d\alpha d\beta . \tag{A2}$$

To find which trajectories intersect the surface of the star, consider the intersection of a photon trajectory with the plane through the center of the star perpendicular to the radial direction in the local rest frame of the star. A trajectory which reaches the observer at $t = t_0$ with $\alpha = \alpha_k + \delta\alpha$, $\beta = \beta_k + \delta\beta$ intersects this plane at the coordinate position $\phi = \phi_s + \delta\phi$, $\theta = \pi/2 + \delta\theta$, $r = r_s$, $t = t_s + \delta t$, to first order in the deviation from the standard trajectory. The spatial displacement of the point of intersection from the center of the star in the local rest frame is

$$\epsilon^{(r)} = \Lambda^{(r)}{}_\alpha \delta x^\alpha = 0 , \tag{A3}$$

$$\epsilon^{(\theta)} = \Lambda^{(\theta)}{}_\alpha \delta x^\alpha = r_s \delta\theta , \tag{A4}$$

$$\epsilon^{(\phi)} = \Lambda^{(\phi)}{}_\alpha \delta x^\alpha = \frac{{r_s}^{1/2} + 1}{[{r_s}^2 + 2{r_s}^{3/2}]^{1/2}} [({r_s}^{3/2} + 1)\delta\phi - \delta t] . \tag{A5}$$

Let the unit tangent vector to the photon trajectory in the three-space of the local rest frame be

$$k^{(a)} = p^{(a)}/p^{(0)} , \tag{A6}$$

where $p^{(\alpha)}$ is the momentum four-vector in the local rest frame. Let ψ be the angle between $k^{(a)}$ and $\epsilon^{(a)}$. The photon trajectory intersects the star if and only if

$$|\epsilon|^2 \sin^2 \psi < b^2 . \tag{A7}$$

Since $\cos^2 \psi = (\epsilon^{(a)}k^{(a)})^2/|\epsilon|^2|k|^2$, the allowed range of $\epsilon^{(\theta)}$ and $\epsilon^{(\phi)}$ is such that

$$(\epsilon^{(\phi)})^2(1 - (k^{(\phi)})^2) + (\epsilon^{(\theta)})^2(1 - (k^{(\theta)})^2) - 2k^{(\theta)}k^{(\phi)}\epsilon^{(\theta)}\epsilon^{(\phi)} < b^2 . \tag{A8}$$

This is an ellipse in the $(\epsilon^{(\phi)}, \epsilon^{(\theta)})$ parameter space with an area

$$\pi b^2[1 - k^{(\theta)2} - k^{(\phi)2}]^{-1/2} = \pi b^2/k^{(r)} . \tag{A9}$$

Since

$$p_r = [R(r_s)]^{1/2}/(r_s - 1)^2 , \tag{A10}$$

$$k^{(r)} = g[R(r)]^{1/2}/r_s(r_s - 1) . \tag{A11}$$

The area in the (α, β)-plane corresponding to the above area in the $(\epsilon^{(\theta)}, \epsilon^{(\phi)})$-plane is

$$\iint d\alpha d\beta = \left|\frac{\partial(\alpha, \beta)}{\partial(\epsilon^{(\phi)}, \epsilon^{(\theta)})}\right| \pi b^2 \frac{r_s(r_s - 1)}{g} [R(r_s)]^{-1/2} . \tag{A12}$$

The Jacobian is most easily evaluated in stages. First, note that

$$\epsilon^{(\phi)} = \frac{(r_s^{1/2} + 1)(r_s^{3/2} + 1)}{[r_s^2 + r_s^{3/2}]^{1/2}} \delta\phi^* , \tag{A13}$$

$$\phi^* = \phi - \Omega_s t . \tag{A14}$$

Thus

$$J_1 \equiv \left|\frac{\partial(\delta\phi^*, \delta\theta)}{\partial(\epsilon^{(\phi)}, \epsilon^{(\theta)})}\right| = \frac{(r_s^2 + r_s^{3/2})^{1/2}}{r_s(r_s^{1/2} + 1)(r_s^{3/2} + 1)} . \tag{A15}$$

From equations (28a, b),

$$J_3 \equiv \left|\frac{\partial(\alpha, \beta)}{\partial(\lambda, q)}\right| = \frac{q}{\sin \theta_0 [q^2 + \cos^2 \theta_0 - \lambda^2 \cot^2 \theta_0]^{1/2}} . \tag{A16}$$

This leaves

$$J_2 \equiv \left|\frac{\partial(\delta\phi^*, \delta\theta)}{\partial(\lambda, q)}\right| \tag{A17}$$

to be evaluated by perturbing to first order equations (24)–(26) governing the photon trajectories. The perturbations are carried out keeping ϕ_0, θ_0, t_0 fixed at one end of the trajectory and r fixed equal to r_s at the other end, while varying λ or q. We obtain

$$\frac{\partial\theta}{\partial\lambda} = q \int_{\pi/2}^{\theta_0} \frac{\lambda \cot^2 \theta}{[\Theta(\theta)]^{3/2}} d\theta - q \int_{r_s}^{\infty} \frac{r[(r - 2)\lambda + 2]}{[R(r)]^{3/2}} dr , \tag{A18}$$

$$\frac{\partial\theta}{\partial q} = -q^2 \int_{\pi/2}^{\theta_0} \frac{d\theta}{[\Theta(\theta)]^{3/2}} - q^2 \int_{r_s}^{\infty} \frac{(r - 1)^2}{[R(r)]^{3/2}} dr , \tag{A19}$$

$$\frac{\partial\phi}{\partial\lambda} = -\int_{\pi/2}^{\theta_0} \frac{[q^2 + \cos^2 \theta) \cot^2 \theta}{[\Theta(\theta)]^{3/2}} d\theta - \int_{r_s}^{\infty} \frac{r^4 - q^2(r - 1)^2}{[R(r)]^{3/2}} dr , \tag{A20}$$

$$\frac{\partial\phi}{\partial q} = \frac{\partial\theta}{\partial\lambda}, \tag{A21}$$

$$\frac{\partial t}{\partial\lambda} = -\int_{\pi/2}^{\theta_0} \frac{\lambda\cos^2\theta\cot^2\theta}{[\Theta(\theta)]^{3/2}}\,d\theta - \int_{r_s}^{\infty} \frac{\lambda r^4 + 2q^2 r}{[R(r)]^{3/2}}\,dr, \tag{A22}$$

$$\frac{\partial t}{\partial q} = q\int_{\pi/2}^{\theta_0} \frac{\cos^2\theta}{[\Theta(\theta)]^{3/2}}\,d\theta - q\int_{r_s}^{\infty} \frac{[r^4 + r^2 + 2r - 2\lambda r]}{[R(r)]^{3/2}}\,dr. \tag{A23}$$

Then

$$\frac{\partial\delta\phi^*}{\partial\lambda} = \frac{\partial\phi}{\partial\lambda} - \Omega_s\frac{\partial t}{\partial\lambda}, \qquad \frac{\partial\delta\phi^*}{\partial q} = \frac{\partial\phi}{\partial q} - \Omega_s\frac{\partial t}{\partial q}. \tag{A24}$$

The sign of q in equations (A18)–(A23) is positive if θ increases along the trajectory near the star.

If $q = 0$, so the unperturbed trajectory is in the equatorial plane, then $J_3 = 1$, and equations (A18)–(A24) are replaced by

$$\frac{\partial\theta}{\partial\lambda} = \frac{\partial\phi}{\partial q} = \frac{\partial t}{\partial q} = 0, \tag{A25}$$

$$\frac{\partial\theta}{\partial q} = (\lambda^2 - 1)^{-1/2}\sin\left[(\lambda^2 - 1)^{1/2}\int_{r_s}^{\infty}\frac{dr}{[R(r)]^{1/2}}\right], \tag{A26}$$

and

$$\frac{\partial\delta\phi^*}{\partial\lambda} = -(1 - \Omega_s\lambda)\int_{r_s}^{\infty}\frac{r^4 dr}{[R(r)]^{3/2}}. \tag{A27}$$

Putting everything together,

$$\iint d\alpha d\beta = \pi b^2\frac{r_s(r_s - 1)}{g[R(r_s)]^{1/2}}J_1 J_2^{-1} J_3. \tag{A28}$$

The ratio of the observed flux to the Newtonian flux $L/4\pi r_0^2$ is

$$F_0/F_N = g^3\frac{r_s(r_s - 1)}{[R(r_s)]^{1/2}}J_1 J_2^{-1} J_3. \tag{A29}$$

The interpretation is clearest when the observer is in the equatorial plane. Then

$$F_0/F_N = [g^4]\left|[R(r_s)]^{1/2}\int_{r_s}^{\infty}\frac{r^4 dr}{[R(r)]^{3/2}}\right|^{-1} \times\left|(\lambda^2 - 1)^{-1/2}\sin\left[(\lambda^2 - 1)^{1/2}\int_{r_s}^{\infty}\frac{dr}{[R(r)]^{1/2}}\right]\right|^{-1}. \tag{A30}$$

The first factor in equation (A30) is the relativistic correction to the surface brightness of the image. The shape of the image is an ellipse, with principal axes parallel and perpendicular to the equatorial plane. The second factor gives the relativistic correction to the extension of the image parallel to the plane. This factor can be much less than unity if the trajectory spirals close to the circular photon orbit, at which $R(r)$ has a double zero. It can never be much greater than unity. The third factor is responsible for

all gravitational-lens effects in the equatorial plane. Whenever the argument of the sine is a multiple of π, this factor is *infinite*, corresponding to an infinite relative extension of the image perpendicular to the equatorial plane. The orbits with $\lambda^2 < 1$ are defocused, since then the sine becomes a hyperbolic sine.

REFERENCES

Ames, W. L., and Thorne, K. S. 1968, *Ap. J.*, **151**, 659.
Bardeen, J. M. 1970, *Nature*, **226**, 64.
Bardeen, J. M., Press, W. H., and Teukolsky, S. 1972, *Ap. J.*, **178**, 347.
Campbell, G. A., and Matzner, R. A. 1973, *Phys. Rev.*, to be published.
Carter, B. 1968, *Phys. Rev.*, **174**, 1559.
Lindquist, R. W. 1966, *Ann. Phys. (N.Y.)*, **37**, 487.
Lynden-Bell, D. 1969, *Nature*, **223**, 690.
Lynden-Bell, D., and Rees, M. J. 1971, *M.N.R.A.S.*, **152**, 461.
Misner, C. W., Thorne, K. S., and Wheeler, J. A. 1973, *Gravitation* (San Francisco: W. H. Freeman & Co.) (in press).
Partridge, R. B. 1971, *Phys. Rev. Letters*, **26**, 912.
Peters, P. C. 1964, *Phys. Rev.*, **136**, B1224.
Podurets, M. A. 1965, *Soviet Astr.—AJ*, **8**, 868.
Ruffini, R., and Wheeler, J. A. 1971, in *The Significance of Space Research for Fundamental Physics*, ed. A. F. Moore and V. Hardy (Paris: European Space Research Organization).
Shakura, N. I., and Sunyaev, R. A. 1972, preprint.
Weber, J. 1970, *Phys. Rev. Letters*, **25**, 180.
Webster, B. L., and Murdin, P. 1972, *Nature*, **235**, 37.
Wolfe, A. M., and Burbidge, G. R. 1970, *Ap. J.*, **161**, 419.